Strain-induced band-to-band Fermi level tuning in II-VI and III-V antiphase boundaries

Lipin Chen, Zewen Chen, Jinshi Zhao, Laurent Pedesseau, C. Cornet

Strain-induced band-to-band Fermi Level Tuning in II-VI and III-V Antiphase Boundaries

Lipin Chen[1*], Zewen Chen[1], Jinshi Zhao[1], Laurent Pedesseau[2] and Charles Cornet[2*]

[1]*Tianjin Key Laboratory of Film Electronic & Communicate Devices, School of Integrated Circuit Science and Engineering, Tianjin University of Technology, Tianjin 300384, China*

[2]*Univ Rennes, INSA Rennes, CNRS, Institut FOTON – UMR 6082, F-35000Rennes, France*

Here, we investigate and analyze the electronic properties of ladder- and zigzag-patterned antiphase boundaries (APB) in II-VI and III-V semiconductors based on first-principle calculations performed on ZnS and InP. From the bandstructure analysis on these configurations, we evidence a direct correlation between Fermi levels positioning and the bond length in ladder-patterned APBs. The changes on the APB bond lengths and electronic properties from III-V to II-VI ladder APBs are discussed based on the charges and atoms electronegativity. We then show how the specific atomic configuration of the zigzag-patterned and ladder-patterned APBs differ from the point of view of force accommodation. As a result, ladder-patterned APBs are found to be much more sensitive to any change of the stress or the chemical environment. We finally demonstrate that a small change in the APB bond length deeply modifies the bandstructure and optoelectronic properties of the systems (for both III-V and II-VI semiconductors), with possible n- and p-doping type inversion, thus opening the way towards APB-engineered photoelectric devices.

I. INTRODUCTION

Epitaxial integration of III-V (or II-VI) semiconductors on Si substrate [1,2], can combine the benefits of both Si (e.g., earth abundance, low cost, and prevalence in the electronic and photovoltaic industries) and III-V (or II-VI) semiconductors (excellent optoelectronic performances), which have raised great interest for integrated photonics [3,4], solar cells [5,6], and solar water splitting [7,8] for a long time. Antiphase boundaries (APB) are typical 2D structural defects in epitaxial material on Si, which consist of homovalent bonds and have been considered for many years as detrimental defects for devices without a clear picture of their optoelectronic contribution in the sample. Recent works revealed that the reality turns out to be more complex and these structural defects can also provide additional degrees of freedom for developing new devices [9–11].

The band structures and optoelectronic properties of various III-V APBs have been thoroughly studied in recent years [9–12]. These experimental and theoretical works revealed that APBs can follow several different atomic configurations which strongly impact their optoelectronic properties. Firstly, the band structure and optical properties of III-V stoichiometric {110} APB were clarified [11,13], which show that the electronic band gap is reduced by two-dimensional (2D) electronic localization. Furthermore, an intrinsic and strong electron-phonon coupling was evidenced around the stoichiometric APBs from the analysis of the photoluminescence spectra [11]. Besides, the optoelectronic properties of non-stoichiometric APBs were investigated for InP, GaAs, GaP and GaSb. It was proved that these APBs introduce metallic states inside the semiconductor matrix, giving rise to a hybrid III-V/Si semiconducting/semimetallic structure, which facilitates carriers extraction and contributes to good transport and ambipolar properties [10]. Strong influence of APB

configurations on Fermi level positioning and thus on band lineups and space charge area have been also evidenced in GaP/Si samples based on coherent phonon spectroscopy [14]. Very recently, a first coherent picture of their optoelectronic properties was proposed [9], showing that all these intriguing properties are fundamentally related to their atomic configuration where atoms can be bonded through ladder patterns, zigzag patterns or a combination of the two [9]. In the case of a ladder pattern, APB atoms are bonded to one similar atom, and three different ones. In the case of a zigzag pattern, APB atoms are bonded to two similar atoms, and two different ones. This changes drastically the charge distribution in these objects. This finding led to the proposition of a classification for all the possible APBs bandstructures, together with the description of the associated Fermi levels and their possible use in optoelectronic devices [9].

Overall, beyond the structural defect picture depicted in different studies, these works demonstrated that APBs are 2D homovalent singularities, composed of different rows of 1D stacks of atoms bonded in specific configurations, which symmetry properties differ from the bulk ones, leading to unique optoelectronic properties. Their use in optoelectronic devices becomes more and more realistic as recent experimental and theoretical works clarified (i) their formation through the coalescence of 3D monophase islands [1,15], (ii) the physical processes involved in their propagation during the growth [15,16] and (iii) the experimental control of their distribution in the sample (Antiphase Domain burying or demonstration of a 1D quasi-periodic array of APDs) [16,17]. Thus, further investigations on the physical properties of APBs are of great practical importance, for the development of APB-engineered III-V(or II-VI)/Si epitaxial materials and devices.

Up to now, optoelectronic properties of APBs have been carefully analyzed for weakly polar III-V epitaxial materials. As compared to III-V semiconductors, II-VI semiconductors are significantly more polar, implying that the electric field between atoms is more intense. For this reason, the impact of APBs on the physical properties of these materials, which was not studied previously to our knowledge, is expected to be even stronger. In the present work, we study and analyze, the structural and electronic properties of nonstoichiometric pure zigzag- and ladder-patterned APBs (called zigzag and ladder APBs for short) in Zinc blende ZnS based on first-principle calculations. Besides, by comparing the APBs in ZnS and InP matrixes, we particularly highlight the strong influence of the bond length of ladder APBs on the electronic properties, and doping type.

II. STRUCTURE AND COMPUTATIONAL DETAILS

The atomic structures of the zigzag and ladder APBs are shown in Figure 1a and Figure 1c schematically. On these drawings, the Si (001) substrate has been added for clarity, but is not included in the calculations. Non-stoichiometric ladder and zigzag APBs are specifically divided into two types, corresponding to extreme configurations: one with only goup-II atoms (*i.e.* zigzag:Zn-Zn APB and ladder:Zn-Zn APB) and the other one with only group-VI atoms (*i.e.* zigzag:S-S APB and ladder:S-S APB). The corresponding 3D APB bond configurations are displayed in Figure 1b and Figure 1d, where the zigzag and ladder pattern are isolated for clarity [9].

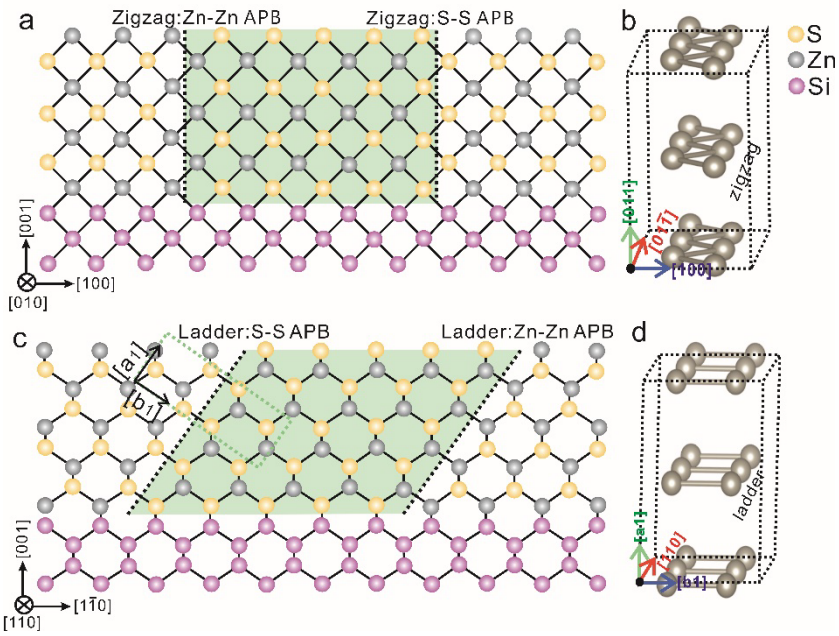

Figure 1: Schematic of non-stoichiometric zigzag (a-b) and ladder (c-d) APB atomic configurations in the Zinc blend ZnS on the Si (001) substrate.

The zigzag and ladder APB atomic structures for calculations are built by using VESTA software. These structures belong to the Pmma and P-3m1 space group, respectively. In order to study the APB singularities separately, slabs with specific APB in the middle of the structures were built by adding vacuum on both truncated sides (left top and right). Each truncated surface has been passivated with fictitious hydrogen atoms (as in previous studies [9,10]) to avoid localized surface states, as shown in the supplemental materials [18]. $1s^{0.5}$ and $1s^{1.5}$ were used as valence electrons for the fictitious H* with a net charge of 0.5e and 1.5e to compensate the VI and II elements, respectively. The thicknesses of the vacuum regions are large (around 25Å) to reduce interaction between the slab surfaces (as explained in ref. [9]). The standard generalized gradient approximation (GGA) parameterized by Perdew-Burke-Ernzerhof (PBE) [19] was used for structure optimization and the structures were relaxed until the Hellmann-Feynman forces on the atoms are less than 10^{-4} eV/Å. The energy cutoff was set to 500 eV.

The band structure calculations were performed with the projector augmented-wave method [20] based on Heyd–Scuseria–Ernzerhof (HSE) hybrid functionals [21,22]. The accuracy of HSE band structure calculation was firstly confirmed by the calculation result of ZnS zinc blende structure with 3.6 eV bandgap (see the supplemental materials [18]), which shows good agreement with the experimental data [23]. We note that, some prior approaches with self-interaction corrections [24,25] may be more efficient to do the APB band structure calculations than expensive HSE functionals in term of computational accuracy and cost, which could be very interesting for us to check in future work. The 3D band structures and total density of states (DOS) were performed by generating *ab initio* tight-binding Hamiltonians from the maximally localized Wannier functions within HSE functional [26], as implemented in Wannier Tools package [27]. The 3D band structures are calculated with kz=0 and the z axis of the reciprocal space corresponds to the crystallographic directions perpendicular to the different APB planes. Besides, the DOS calculations are performed with dense k points (ka>420Å, the length of each lattice vector (a) multiplied by the number of k

points in this direction (k) is larger than 420 Å). For this study, the Bloch wave functions were projected onto the s, p, and d (s and p) atomic orbitals of Zn (S). Besides, the band structures of different strained configurations with various APB bond lengths are performed with the GGA functional.

To identify the contribution of the APB atoms to the electronic states, APB atom-projected band structures on APB atoms are studied, where the color scale indicates the spatial localization of the electronic state in the APB plane. The color map from blue to red underlines the increase of localization effect of the states at the APB atoms. The dark-blue bands are thus not localized near the APB, and mainly come from the bulk atoms (called bulklike bands in the following parts).

III. RESULTS AND DISCUSSION

Firstly, the band structures of ZnS zigzag APBs are calculated along the following k-path X(-0.5,0,0)-Γ(0,0,0)-X(0.5,0,0) including the correction of the HSE functional, where the x axis of the reciprocal space corresponds to the $[01\bar{1}]$ crystallographic direction (Fig.1b). Note that the common k-paths chosen in all cases for comparison lie in the APB plane to illustrate the effects of the 2D electronic dispersion. For the 3D band structures, we focus on the $k_{x,y}$ plane with k_z=0, corresponding to the APB plane.

The APB atom-projected band structures of zigzag:Zn-Zn and zigzag:S-S APBs are shown in Figure 2a and c, respectively, and the corresponding 3D band structures and density of states are shown in Figure 2b and d. For comparison, the results obtained in our previous work [9] on zigzag:In-In and zigzag:P-P are also displayed in Fig.2e-h. It can be observed that, as in the case of zigzag:V-V and zigzag:III-III APBs, zigzag:S-S and zigzag:Zn-Zn APBs also introduce interesting APB localized metallic states connecting the bulklike VBs and CBs and, hence, closing the bandgap. The APB localized metallic states exhibit similar shape. Besides, similarly, zigzag:S-S and zigzag:Zn-Zn APBs also show relatively high and low Fermi energy levels, respectively, and behave as n-doped and p-doped semiconductors, respectively. Therefore, in the same way as non-stoichiometric III-V zigzag APBs, II-VI zigzag APBs may induce in-plane lateral nano-scale p-n junctions and that can potentially be used for carrier separation and extraction in light harvesting devices (e.g. for solar cells or solar water splitting devices) [9,10].

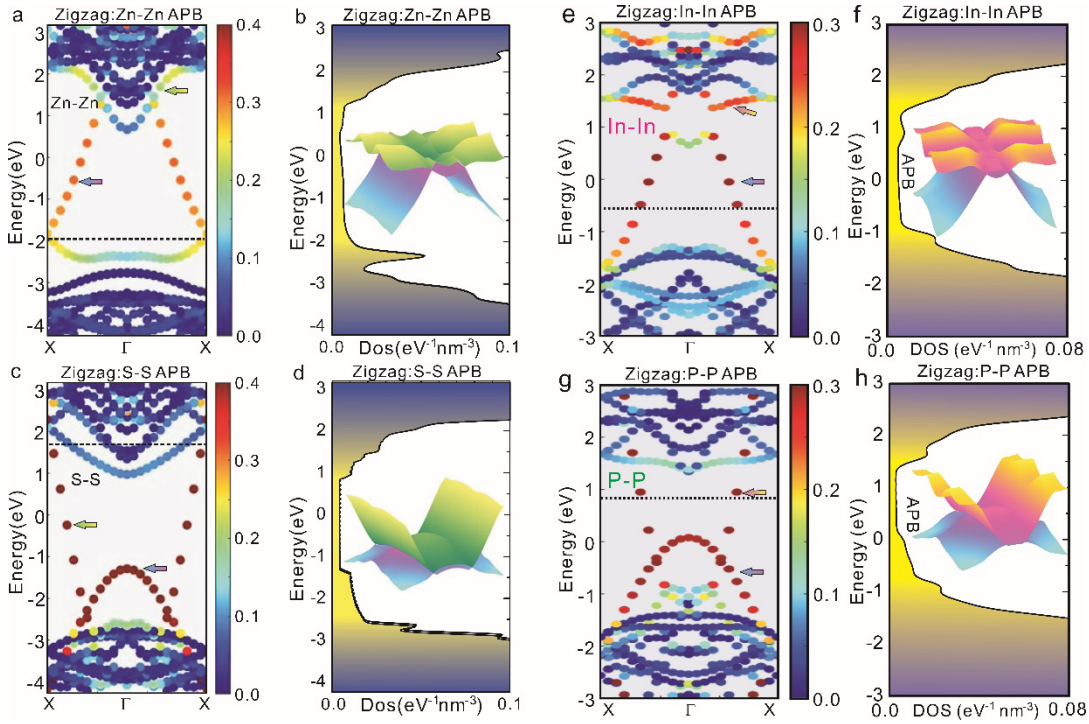

Figure 2: Band structure and DOS calculations of zigzag:Zn-Zn (a,b), zigzag:S-S (c,d), zigzag:In-In (e,f) and zigzag:P-P APBs (g,h). (a,c,e,g) Atom-projected band structures of zigzag:Zn-Zn APB on II-II APB atoms (a), zigzag:S-S APB on VI-VI APB atoms (c), zigzag:In-In APB on III-III APB atoms (e) and zigzag:P-P APB atoms on V-V APB atoms (g). (b,d,f,h) 3D band structures (at $k_z = 0$ plane) and density of states. The insets show the 3D band structures for zigzag:Zn-Zn (b), zigzag:S-S (d), zigzag:In-In (f), and zigzag:P-P(h) APBs, corresponding to the principal bands localized around the APB, which are marked by the arrows in (a), (c), (e), (g). InP zigzag APBs bandstructures are equivalent to the ones presented in ref. [9].

Then, the band structures of ladder-patterned APBs were investigated. Figure 3a and Figure 3c show the atom-projected band structures of the ladder: Zn-Zn APB and ladder:S-S APB on the Zn-Zn and S-S APB atoms, respectively, where the x axis of the reciprocal space corresponds to the [110] crystallographic direction (Fig.1d). The 3D band structure and density of states of the ladder:Zn-Zn APB and ladder:S-S APB are shown in Figure 3b and d, respectively. Again, for comparison, the band structure and DOS calculations of ladder:In-In and ladder:P-P APBs similar to previous works [9] are also displayed in Fig.3e-h.

In this case, the ladder-patterned III-V and II-VI APBs show quite different features. As discussed in a previous work [9], the ladder:III-III and V-V APBs introduce localized APB states both at the top of the bulklike valence bands (VBs) and at the bottom of the bulklike conduction bands (CBs). The localized APB states mix with the bulklike states with a large energy dispersion (as shown in 3D band structure images). The situation is different for II-VI APBs. For the ladder:II-II and VI-VI APBs, the localized APB states are very localized (very flat) throughout the k-path which is the signature of a strong localization effect. This is highlighted by the overall view based on the 3D bands (the green-to-yellow 3D bands in Fig.3b and Fig.3d). Indeed, there are obvious energy gaps between the localized APB states and the bulklike CB and VB states. This means that the ladder:Zn-Zn and ladder:S-S APBs introduce flat partially filled intermediate bands (IBs) in the bulklike bands,

which could be of interest for solar energy harvesting devices [28,29], as the partially filled IBs can also permit the absorption of low-energy photons to pass the electrons from the VB to the partially filled IB and from there to the CB, except of the absorption of relative high-energy photons to excite the electron from the VB to the CB directly [28,29].

Moreover, it is demonstrated that the Fermi energy levels cross the localized APB states for the two configurations, with a relatively high and low Fermi energy levels for the ladder: Zn-Zn and ladder:S-S APBs, respectively. This means the ladder: Zn-Zn and ladder:S-S APBs behave as n-doped and p-doped semiconductors, respectively, which is the opposite situation as compared to the ladder:III-III and ladder:V-V APBs. Indeed, the ladder: In-In and ladder:P-P APBs exhibit low and high Fermi energy levels, respectively.

To summarize briefly, non-stoichiometric ZnS zigzag-patterned APBs show similar electronic properties than their corresponding III-V cases [9,10]. On the contrary, non-stoichiometric ZnS ladder-patterned APBs exhibit quite different characteristics, in terms of band shape of the localized APB states and of positioning of the Fermi energy levels, even though non-stoichiometric zigzag and ladder APBs have a similar composition (which are composed of pure II (III) or pure VI (V) atoms).

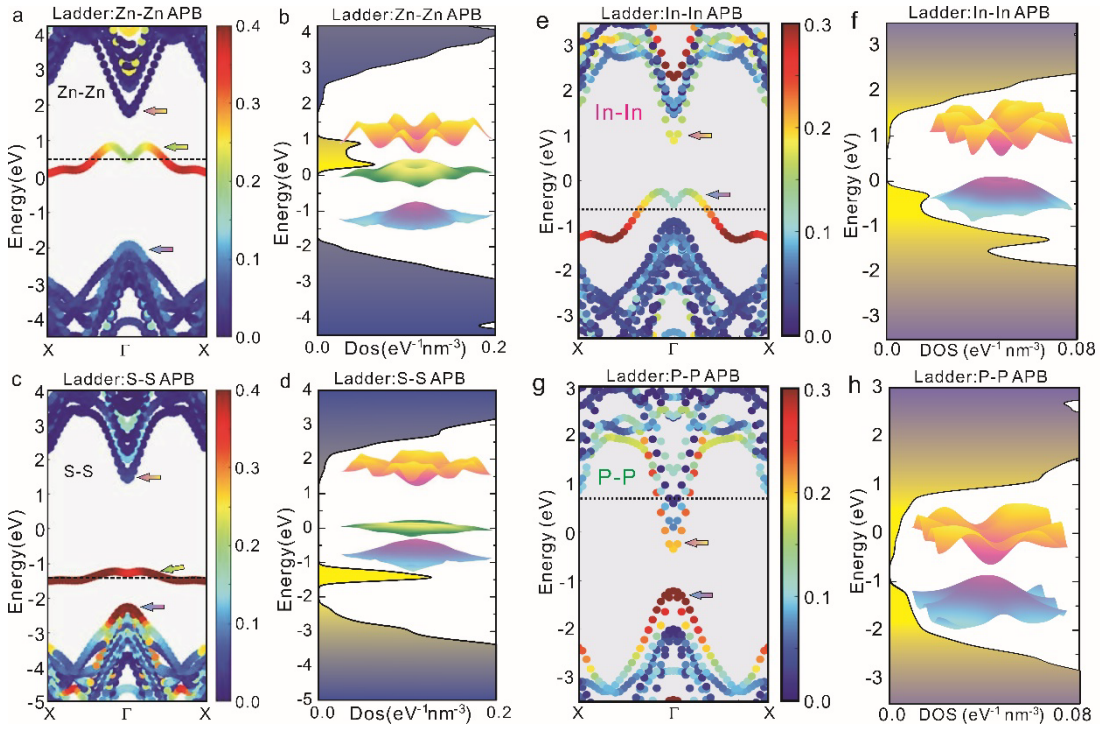

Figure 3: Band structure and DOS calculations of ladder:Zn-Zn (a,b), ladder:S-S (c,d), ladder:In-In (e,f) and ladder:P-P APBs (g,h). Atom-projected band structures of ladder:Zn-Zn APB on II-II APB atoms (a), ladder:S-S APB on VI-VI APB atoms (c), ladder:In-In APB on III-III APB atoms (e) and ladder:P-P APB atoms on V-V APB atoms (g). (b,d,f,h) 3D band structures (at $k_z = 0$ plane) and density of states. The insets show the 3D band structures for ladder:Zn-Zn (b), ladder:S-S (d), ladder:In-In (f), and ladder:P-P (h) APBs, corresponding to the main bands localized around the APB, which are marked by the arrows in (a), (c), (e), (g). For the ladder:Zn-Zn (b), ladder:S-S (d) APBs, the bulklike bands neighboring around the APB localized bands are also extracted. InP ladder-APBs bandstructures are equivalent to the ones presented in ref. [9].

To understand the above observations, the influence of the bond length of each II-II, VI-VI, III-III, and V-V doublets inside the APBs is investigated in the following. The APB bond lengths of zigzag and ladder ZnS and InP APBs after relaxation are summarized in Table 1, together with the corresponding electronic behavior (n- or p-type). The n-type and p-type electronic behavior correspond to the case where the Fermi energy level is closer to the bulklike conduction band (CB) and valence band (VB), respectively. In Table 1, it is shown that the zigzag InP APBs, zigzag ZnS APBs, and ladder InP APBs, present the same behavior: the bond length of the cationic APBs (*i.e.* zigzag:In-In, zigzag:Zn-Zn and ladder:In-In APBs) is relatively long and the bond length of the corresponding anionic APB (*i.e.* zigzag:P-P, zigzag:S-S and ladder:P-P APBs) is relatively short. Table 1 also shows that, for these three kinds of APBs, the cationic APBs (*i.e.* zigzag:In-In, zigzag:Zn-Zn and ladder:In-In APBs) have relatively low Fermi energy levels and thus display p-type electronic behavior. On the contrary, anionic APBs (i.e. zigzag:P-P, zigzag:S-S and ladder:P-P APBs) have relatively high Fermi energy level and thus exhibit n-type electronic characteristics. The situation is different for the ladder ZnS APBs: the bond length of ladder: S-S APB is significantly longer than the ones of zigzag:S-S, zigzag:P-P, and ladder: P-P APBs (Table 1). On the contrary, the bond length of ladder: Zn-Zn APB becomes relatively short. Therefore, the surprising Fermi energy positioning of ladder:Zn-Zn and ladder:S-S APBs should be directly correlated to the anomalous change of the APB bond lengths. Indeed, the shorter APB bond length is, the higher charge density obtained between the APB atoms, and subsequently a higher Fermi energy level is expected. This shows good consistency to the classical free electron theory [30,31], which predicts that the variation of Fermi energy level depends on the electron or hole concentration of the doping or defect atoms. In order to understand the results more clearly, there are two questions needed to be analyzed: (1) With the same atomic structures, why the II-VI and III-V ladder APBs show such huge differences in APB bond lengths and electronic behavior? (2) With similar compositions, why only ladder APBs display such differences, while zigzag APBs do not, with the change of elements (from III to II or from V to VI)?

Table 1. APB bond lengths of zigzag and ladder APBs based on ZnS and InP matrix together with the electronic properties (n-type and p-type electronic property corresponding to the case of Fermi energy level closer to bulklike conduction bands (CBs) and valence bands (VBs), respectively).

APB type	Zigzag-patterned APBs				Ladder-patterned APBs			
	S-S	Zn-Zn	P-P	In-In	S-S	Zn-Zn	P-P	In-In
Electronic behavior	n-type	p-type	n-type	p-type	p-type	n-type	n-type	p-type
Bond length (Å)	2.10	2.60	2.31	2.92	2.83	2.48	2.21	2.86

To clarify the question 1, a careful analysis of the electron distribution and bonding for ladder InP (Fig. 4(a,b)) and ZnS (Fig. 4(c-e)) APBs is proposed. We consider anionic APBs (*i.e.* ladder:P-P and S-S APBs) as an example, as shown in Fig.4. Firstly, for the InP semiconductor, the In-P bonds are

mainly covalent. From the charge point of view, each In-P bond forms by 0.75e from In atom and 1.25e from P atom (as shown in Fig.4a) and these electrons are shared by In and P atoms. For the ladder:P-P APB, each P APB atom has one bond connected to one other APB atom and as well as three bonds connected to three bulk In atoms. For the P-P APB bond, each P APB atom shares 1.25e (Fig.4b), which leads to an excess of 0.5e per P APB atom. This is the reason why the P-P ladder APB exhibits n-type electronic behavior [9]. Whereas, for the ZnS semiconductor, as the difference of the electronegativity between S and Zn is much larger than P and In (electronegativity: S:2.58; Zn:1.65; P:2.19; In: 1.78), Zn-S bonds are more ionic. The electrons forming the Zn-S bond (0. 5e of Zn atom and 1.5e of S atom) are attracted much more strongly by S atom than by the Zn atom, which leads to obvious electronegativity for S atoms and electropositivity for Zn atoms. Therefore, in the ZnS semiconductor, each S atom will be mainly attracted by surrounded four Zn atoms (Fig.4c), and the S atoms will be stabilized by cancelling the four attractive forces out each other. While for the ladder:S-S APB, firstly, we assume that the two parts of 1.5e from the two S APB atoms are superimposed and shared by the two S APB atoms (Fig.4d) as in the case of ladder: P-P APB(Fig.4b). In this case, the two S APB atoms should be very close due to the strong electronegativity of S [32,33]. But, on the other hand, if we analyze the force state of the S APB atoms, we can find that there is a strong repulsive interaction between the two S APB atoms [33]. Meanwhile, the bulk Zn atoms on the other side attract the S APB atom, which leads to a destabilization of S APB atoms (as shown in Fig.4d). Therefore, to reach a stable condition, the distance between the two S APB atoms will increase. Finally, the case of Fig.4e is expected to be obtained, where the distance between the two S APB atoms is large and the two parts of the 1.5e of two S APB atoms almost do not overlap. In this case, each S APB atom will have a deficit of 0.5e, which shows good agreement with the p-type electronic characteristic of the ladder:S-S APB.

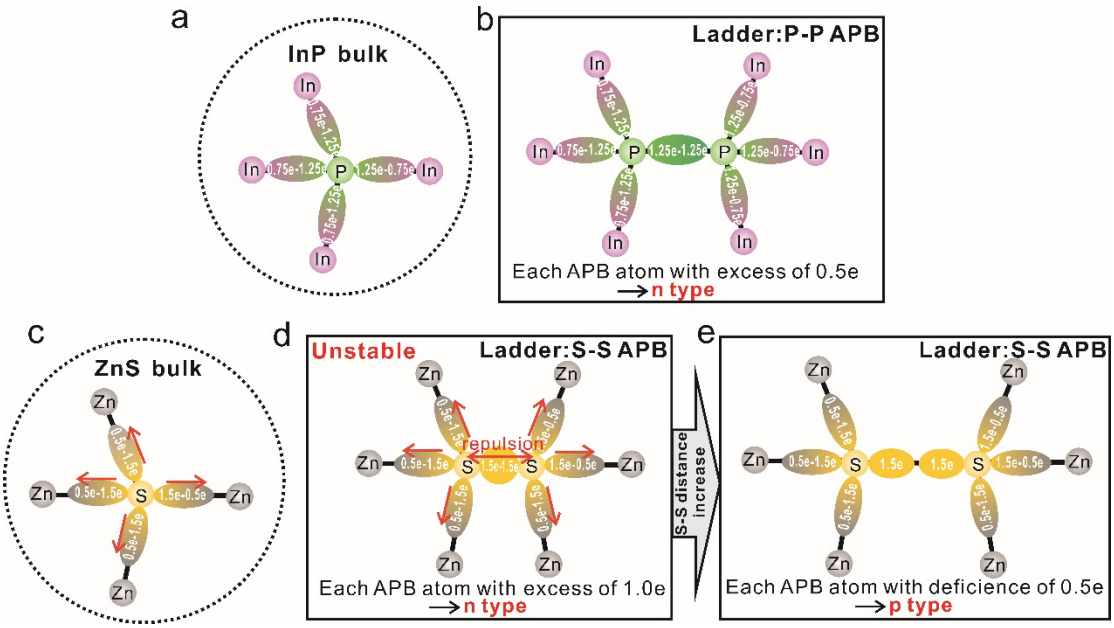

Figure 4: Schematic diagram of electron distribution and bonding for ladder: P-P(a,b) and S-S(c-e) APBs. The red arrows correspond to the directions of forces on S atom by the surrounding atoms.

Besides, to better understand the questions 2, the atomic configurations of the two types of APBs are carefully analyzed. Figure 5 gives the zoomed-in atomic configurations of zigzag-patterned and ladder-patterned APBs. As mentioned above, for the ladder pattern (Fig.5a), each APB atom has only one bond connected with one other APB atom. While, for the zigzag case (Fig.5b), each APB atom has two bonds connected with the other APB atoms, forming an angle θ. Therefore, when elements are changed (e.g. from III(V) to II(VI) atoms), the forces on the APB atoms also change. For the ladder pattern (Fig.5a), the forces on the APB atoms can only be adjusted by the APB bond length. That's why the bond length of ladder VI-VI APB shows a huge change. While, for the zigzag pattern (Fig.5b), the forces on the APB atoms can be adjusted not only by the length of the APB bond, but also by the angle θ, which causes relatively small changes on the APB bond length of zigzag APBs. Indeed, the angle θ for the VI-VI zigzag APB (139°) becomes larger than the one for the V-V zigzag APB (134°). For this reason, the bond length in the ladder pattern is much more impacted by the change of atoms (from III to II or from V to VI) than the zigzag pattern, which fully explains results of Table 1.

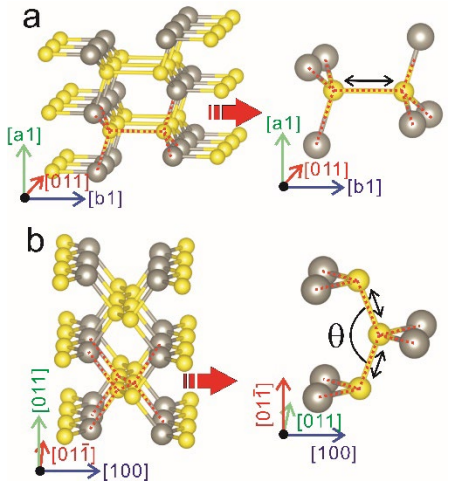

Figure 5: Zoomed-in atomic configurations of ladder (a) and zigzag (b) APBs. For the ladder configuration, each APB atom has only one bond connected with one other APB atom. For the zigzag configuration, each APB atom has two bonds connected with other APB atoms, forming an Angle θ.

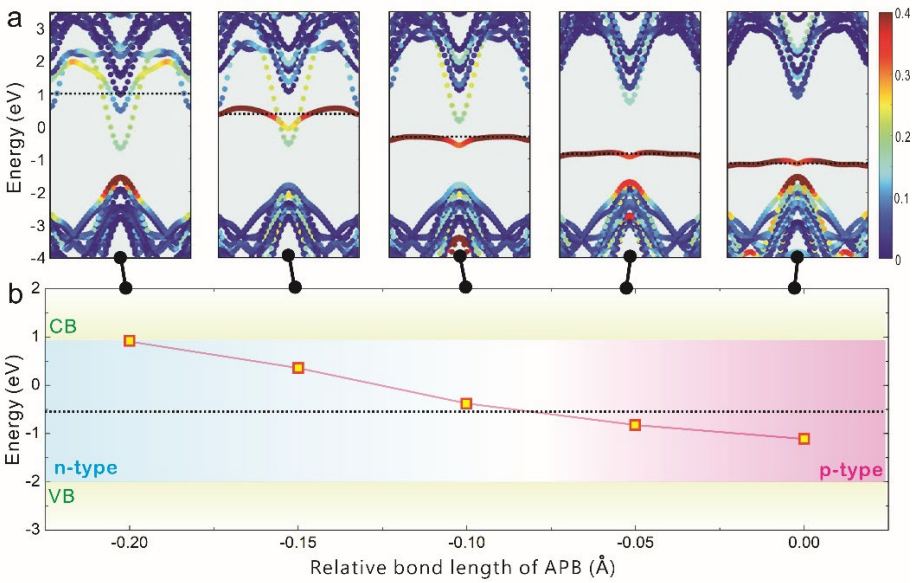

Figure 6: (a) APB atom-projected band structures of different ZnS ladder:S-S APB structures with different APB bond lengths changed manually. (b) Evolution of integrated Fermi energy levels of the different APB structures with the increase of APB bond lengths. The x- axis represents the relative length of the APB bond. The five data points from right to left correspond to structures with reducing the APB bond length by 0.0 Å, 0.05 Å, 0.10 Å, 0.15 Å, and 0.20 Å, respectively. The black dotted line shows the middle of the bandgap and the light-green areas correspond to the valence bands (VB) and conduction bands (CB) of the bulk material without APBs.

To further verify the relationship between the Fermi level energy positioning and the APB bond lengths of the ladder configurations, we performed band structure calculations for different ladder:S-S APB structures as a function of APB bond lengths (note that this procedure corresponds to the introduction of an artificial strain field only for the 2D APB area, but not in the bulk region and more details about the methodology can be obtained in supplemental materials [18]). Results are reported in Fig.6. With the decrease of the APB bond lengths (from the right side to the left side in Fig.6), the positions of the flat APB localized intermediate bands (IB) and Fermi energy levels of ladder:S-S APB increase gradually, thus changing the electronic behavior from p-type to n-type electronic property, which further confirms that the bond length of ladder APB strongly affect the Fermi energy levels. When the APB bond length reduces by 0.2Å from the original structure with full relaxation, the APB localized band joins with the bulk conduction band, similarly to what is observed for the ladder:P-P APB (Fig.3g). Besides, ladder:P-P APB structures with different APB bond lengths have also been investigated (see the supplemental materials [18]), where a similar conclusion can be obtained. This finding not only provides a general framework to predict the optoelectronic properties of antiphase and inversion boundaries in many different materials systems beyond the conventional III-V and II-VI semiconductors, but also opens another degree of freedom for the development of APB-engineered photoelectric devices. Indeed, while intrinsic piezoelectric properties of the material are supposed to be strongly modified by the presence of APBs, the present study shows that the application of a small external stress on a sample containing APBs would lead naturally to consequent Fermi level shifting and a possible inversion of the doping type, thus

modifying its transport properties, its internal lateral built-in electric field and its photo-generated carriers collection capabilities [10]. This large tunability is of great interest for photonic, sensors, electronic or energy applications.

IV. CONCLUSION

In conclusion, we studied and analyzed the electronic band structures of ladder- and zigzag-patterned antiphase boundaries (APBs) in II-VI (ZnS) and III-V (InP) semiconductors by first-principle calculations. As compared to the III-V APBs, we demonstrate that the zigzag II-VI APBs have a similar impact on the band structures, but the ladder II-VI APBs have a different behavior regarding the shape and positioning of the localized APB states. In addition, we have shown that these alterations also affect the positioning of Fermi energy levels passing through the localized APB states, which result from a large change of the ladder-patterned APB bond length. Besides, we demonstrated that the large change of the ladder-patterned APB bond length is closely related to the electronegativity of the elements and the specific atom configuration of the APB. On this basis, we finally showed that a small change in the APB bond length deeply modifies the bandstructure and optoelectronic properties of the systems (for both III-V and II-VI semiconductors), with possible n- and p-doping type inversion, thus opening the way towards adjustable optoelectronic properties of APB-engineered materials, through the application of an external stress on the material.

Acknowledgments:
This research was supported by the French National Research Agency PIANIST Project (Grant No. ANR-21-CE09-0020), the NUAGES Project (Grant No. ANR-21-CE24-0006), the Innovative Talents Promotion Plan in Tianjin (Grant No. 2020TD003) and the Tianjin Technical Expert Project (Grant Nos. 22YDTPJC00390 and 22YDTPJC00530).

References:

[1] I. Lucci, S. Charbonnier, L. Pedesseau, M. Vallet, L. Cerutti, J.-B. Rodriguez, E. Tournié, R. Bernard, A. Létoublon, N. Bertru, A. Le Corre, S. Rennesson, F. Semond, G. Patriarche, L. Largeau, P. Turban, A. Ponchet, C. Cornet, Universal description of III-V/Si epitaxial growth processes, Phys. Rev. Materials. 2 (2018) 060401.

[2] K. Qiu, D. Qiu, L. Cai, S. Li, W. Wu, Z. Liang, H. Shen, Preparation of ZnS thin films and ZnS/p-Si heterojunction solar cells, Materials Letters. 198 (2017) 23–26.

[3] M. Tang, J.-S. Park, Z. Wang, S. Chen, P. Jurczak, A. Seeds, H. Liu, Integration of III-V lasers on Si for Si photonics, Progress in Quantum Electronics. 66 (2019) 1–18.

[4] A.K. Katiyar, A.K. Sinha, S. Manna, S.K. Ray, Fabrication of Si/ZnS Radial Nanowire Heterojunction Arrays for White Light Emitting Devices on Si Substrates, ACS Appl. Mater. Interfaces. 6 (2014) 15007–15014.

[5] M. Feifel, D. Lackner, J. Schön, J. Ohlmann, J. Benick, G. Siefer, F. Predan, M. Hermle, F. Dimroth, Epitaxial GaInP/GaAs/Si Triple-Junction Solar Cell with 25.9% AM1.5g Efficiency Enabled by Transparent Metamorphic AlxGa1−xAsyP1−y Step-Graded Buffer Structures, Solar RRL. 5 (2021) 2000763.

[6] S.S. Yesilkaya, U. Ulutas, H.M.A. Alqader, Effect of Na doping on the properties of ZnS thin films and ZnS/Si heterojunction cells, Materials Letters. 288 (2021) 129347.

[7] M. Alqahtani, S. Sathasivam, L. Chen, P. Jurczak, R. Piron, C. Levallois, A. Létoublon, Y.

Léger, S. Boyer-Richard, N. Bertru, J.-M. Jancu, C. Cornet, J. Wu, I. P. Parkin, Photoelectrochemical water oxidation of GaP 1−x Sb x with a direct band gap of 1.65 eV for full spectrum solar energy harvesting, Sustainable Energy & Fuels. 3 (2019) 1720–1729.

[8] P. Kumar, P. Devi, R. Jain, S.M. Shivaprasad, R.K. Sinha, G. Zhou, R. Nötzel, Quantum dot activated indium gallium nitride on silicon as photoanode for solar hydrogen generation, Commun Chem. 2 (2019) 1–7.

[9] L. Chen, L. Pedesseau, Y. Léger, N. Bertru, J. Even, C. Cornet, Antiphase boundaries in III-V semiconductors: Atomic configurations, band structures, and Fermi levels, Phys. Rev. B. 106 (2022) 165310.

[10] L. Chen, Y. Léger, G. Loget, M. Piriyev, I. Jadli, S. Tricot, T. Rohel, R. Bernard, A. Beck, J. Le Pouliquen, P. Turban, P. Schieffer, C. Levallois, B. Fabre, L. Pedesseau, J. Even, N. Bertru, C. Cornet, Epitaxial III–V/Si Vertical Heterostructures with Hybrid 2D-Semimetal/Semiconductor Ambipolar and Photoactive Properties, Advanced Science. 9 (2022) 2101661.

[11] L. Chen, O. Skibitzki, L. Pedesseau, A. Létoublon, J. Stervinou, R. Bernard, C. Levallois, R. Piron, M. Perrin, M.A. Schubert, A. Moréac, O. Durand, T. Schroeder, N. Bertru, J. Even, Y. Léger, C. Cornet, Strong Electron–Phonon Interaction in 2D Vertical Homovalent III–V Singularities, ACS Nano. 14 (2020) 13127–13136.

[12] O. Rubel, S.D. Baranovskii, Formation Energies of Antiphase Boundaries in GaAs and GaP: An ab Initio Study, International Journal of Molecular Sciences. 10 (2009) 5104–5114.

[13] E. Tea, J. Vidal, L. Pedesseau, C. Cornet, J.-M. Jancu, J. Even, S. Laribi, J.-F. Guillemoles, O. Durand, Theoretical study of optical properties of anti phase domains in GaP, Journal of Applied Physics. 115 (2014) 063502.

[14] K. Ishioka, K. Brixius, A. Beyer, A. Rustagi, C.J. Stanton, W. Stolz, K. Volz, U. Höfer, H. Petek, Coherent phonon spectroscopy characterization of electronic bands at buried semiconductor heterointerfaces, Appl. Phys. Lett. 108 (2016) 051607.

[15] C. Cornet, S. Charbonnier, I. Lucci, L. Chen, A. Létoublon, A. Alvarez, K. Tavernier, T. Rohel, R. Bernard, J.-B. Rodriguez, L. Cerutti, E. Tournié, Y. Léger, M. Bahri, G. Patriarche, L. Largeau, A. Ponchet, P. Turban, N. Bertru, Zinc-blende group III-V/group IV epitaxy: Importance of the miscut, Phys. Rev. Mater. 4 (2020) 053401.

[16] A. Gilbert, M. Ramonda, L. Cerutti, C. Cornet, G. Patriarche, É. Tournié, J. Rodriguez, Epitaxial Growth of III-Vs on On-Axis Si: Breaking the Symmetry for Antiphase Domains Control and Burying, Advanced Optical Materials. 11 (2023) 2203050.

[17] M. Rio Calvo, J.-B. Rodriguez, C. Cornet, L. Cerutti, M. Ramonda, A. Trampert, G. Patriarche, É. Tournié, Crystal Phase Control during Epitaxial Hybridization of III-V Semiconductors with Silicon, Advanced Electronic Materials. 8 (2022) 2100777.

[18] See Supplemental Material for additional information of APB structures build for calculations, band structures of ZnS primitive cell with HSE hybrid functional, methodology used to introduce strain in the APB part, and bandstructures of different ladder P-P APB structures with different APB bond lengths.

[19] J.P. Perdew, K. Burke, M. Ernzerhof, Generalized Gradient Approximation Made Simple, Phys. Rev. Lett. 77 (1996) 3865–3868.

[20] P.E. Blöchl, Projector augmented-wave method, Phys. Rev. B. 50 (1994) 17953–17979.

[21] J. Heyd, G.E. Scuseria, M. Ernzerhof, Hybrid functionals based on a screened Coulomb

potential, The Journal of Chemical Physics. 118 (2003) 8207–8215.
[22] J. Heyd, G.E. Scuseria, Efficient hybrid density functional calculations in solids: Assessment of the Heyd–Scuseria–Ernzerhof screened Coulomb hybrid functional, The Journal of Chemical Physics. 121 (2004) 1187–1192.
[23] A. Jrad, M. Naouai, S. Ammar, N. Turki-Kamoun, Investigation of molybdenum dopant effect on ZnS thin films: Chemical composition, structural, morphological, optical and luminescence surveys, Materials Science in Semiconductor Processing. 130 (2021) 105825.
[24] G. Janesko, Replacing hybrid density functional theory: motivation and recent advances, Chemical Society Reviews. 50 (2021) 8470-8495.
[25] R. Shinde, S. S. Yamijala, B. M. Wong, Improved band gaps and structural properties from Wannier–Fermi–Löwdin self-interaction corrections for periodic systems, Journal of Physics: Condensed Matter. 33 (2020) 115501.
[26] C. Franchini, R. Kováčik, M. Marsman, S.S. Murthy, J. He, C. Ederer, G. Kresse, Maximally localized Wannier functions in LaMnO3 within PBE + U, hybrid functionals and partially self-consistent GW: an efficient route to construct ab initio tight-binding parameters for eg perovskites, J. Phys.: Condens. Matter. 24 (2012) 235602.
[27] Q. Wu, S. Zhang, H.-F. Song, M. Troyer, A.A. Soluyanov, WannierTools: An open-source software package for novel topological materials, Computer Physics Communications. 224 (2018) 405–416.
[28] A. Martí, E. Antolín, C.R. Stanley, C.D. Farmer, N. López, P. Díaz, E. Cánovas, P.G. Linares, A. Luque, Production of Photocurrent due to Intermediate-to-Conduction-Band Transitions: A Demonstration of a Key Operating Principle of the Intermediate-Band Solar Cell, Phys. Rev. Lett. 97 (2006) 247701.
[29] A. Luque, A. Martí, C. Stanley, Understanding intermediate-band solar cells, Nature Photon. 6 (2012) 146–152.
[30] W. A. Harrison, Solid State Theory (Courier Corporation, 1980).
[31] C. Kittel, Introduction to Solid State Physics (Wiley, 1966).
[32] W. Gordy, A relation between bond force constants, bond orders, bond lengths, and the electronegativities of the bonded atoms, The Journal of Chemical Physics. 14 (1946) 305–320.
[33] G.B. Bacskay, J.R. Reimers, S. Nordholm, The Mechanism of Covalent Bonding, J. Chem. Educ. 74 (1997) 1494.